RSC Advances

COMMUNICATION

View Article Online
View Journal | View Issue

Cite this: *RSC Adv.*, 2017, **7**, 821

Received 17th October 2016
Accepted 15th November 2016

DOI: 10.1039/c6ra25337g

www.rsc.org/advances

Triazatruxene radical cation: a trigonal class III mixed valence system†

Tony George Thomas,[a] Sarap Chandra Shekar,[b] Rotti Srinivasamurthy Swathi*[b] and Karical Raman Gopidas*[a]

The highly symmetric and stable triazatruxene radical cation was generated chemically for the first time. The intervalence charge transfer (IV-CT) absorption band of the radical cation was observed at 7500–12 500 cm^{-1}. The IV-CT band exhibited a well-resolved, solvent independent vibrational structure which prompted us to classify the radical cation as a Robin and Day class III IV-CT compound. The assignment was examined in light of two previously reported semi-classical models for three-center IV-CT systems. The triazatruxene radical cation is the first and only example of a three-center class III IV-CT system.

Organic mixed valence systems generally exhibit intervalence charge transfer (IV-CT)[1,2] absorption bands which are amenable to spectroscopic analysis using Marcus–Hush theory.[3–5] Mixed valence systems typically contain two redox centers with different oxidation states which are connected by saturated or unsaturated bridges. Derivatives of phenylenediamine and triarylamine are among the heavily investigated organic mixed valence systems as these compounds have applications as hole-transporting materials in organic light emitting diodes and organic solar cells.[6–12] Herein we report the IV-CT behavior in a trigonally symmetric organic molecule, triazatruxene (TAT, Fig. 1). Because of their intrinsic photophysical, redox and π-stacking properties, derivatives of TAT have potential applications in organic electronics and also in supramolecular chemistry.[13–21] For example, semiconducting discotic liquid crystals with triazatruxenes as central core have exhibited very high hole-mobilities. They also have found applications in organic light emitting diodes, bulk heterojunction solar cells and organic field effect transistors. One electron oxidation of TAT leads to formation of its radical cation $TAT^{\bullet+}$. Electrochemical oxidation of TAT ($R = C_8H_{17}$) and the absorption spectrum of its radical cation are reported.[22]

The 'hole' in $TAT^{\bullet+}$ can, in principle, shuttle among all the three N atoms paving the way for IV-CT, but nothing is known about the IV-CT phenomenon in $TAT^{\bullet+}$. In this paper we report chemical oxidation of TAT to its radical cation and present an analysis of its IV-CT band. Structure of the TAT molecule studied is shown in Fig. 1 ($R = CH_3$). TAT may be regarded as a ring-fused analog of 1,3,5-tris(arylamino)benzene (TAB). It may also be regarded as a trimer of indole or even as a trimer of carbazole sharing a fused benzene ring. Both TAT and TAB have more than two redox active units arranged in non-linear fashion and one- and two-electron oxidation of these systems would lead to multi-dimensional mixed valence systems. EPR investigations have shown that the unpaired electron in the mono-radical cation of a symmetrical derivative of TAB (R = phenyl) is delocalized equally over all the three N atoms at −78 °C.[23] Detailed optical investigations of these systems were not carried out as the radical cations were unstable at room temperature.

TAT was synthesized following a reported procedure.[24,25] Cyclic voltammetry in acetonitrile (ACN) showed oxidation peaks at 0.78 V (reversible) and 1.39 V (irreversible) *vs.* SCE (see ESI†). Previous studies from our group have shown that aromatic amines with $E_{ox} < 1.0$ V can be oxidized to their radical cations by reaction with Cu^{2+} in ACN.[26,27] Likewise we generated

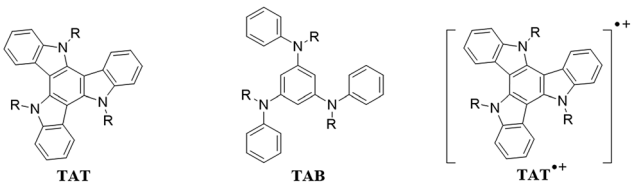

Fig. 1 Structures of TAT, TAB and $TAT^{\bullet+}$.

[a]*Photosciences and Photonics, Chemical Sciences and Technology Division, CSIR-National Institute for Interdisciplinary Science and Technology (CSIR-NIIST), Thiruvananthapuram, India. E-mail: gopidaskr@niist.res.in*

[b]*School of Chemistry, Indian Institute of Science Education and Research, IISER-TVM, Thiruvananthapuram, Kerala, India. E-mail: swathi@iisertvm.ac.in*

† Electronic supplementary information (ESI) available: General experimental procedures, characterization data for TAT, cyclic and square wave voltammograms of TAT, simulated EPR spectrum of $TAT^{\bullet+}$, theoretical details of three-state models, potential energy surfaces of LB model, potential energy surfaces of Cannon model, computational details and EPR spectrum of $TAT^{\bullet+}$ computed using DFT (PDF). See DOI: 10.1039/c6ra25337g

$TAT^{\bullet+}$ (optimized geometry obtained using DFT (B3LYP/6-311G(d,p) level) is shown in Fig. 2A) using one equivalent of Cu^{2+} in ACN. We also generated $TAT^{\bullet+}$ in dichloromethane (DCM) by reacting TAT with one equivalent of $SbCl_5$.

$TAT^{\bullet+}$ was very stable in ACN and DCM solutions and the solutions could be preserved for several hours at room temperature without degradation. Since the second oxidation is irreversible, stability of the product would imply that oxidation of $TAT^{\bullet+}$ to TAT^{2+} has not occurred under the reaction conditions employed.

TAT/Cu^{2+} (1 : 1) solution in ACN exhibited a single broad line EPR signal (Fig. 2B) with a spectral width of ~38 G, and *g* value of 2.01, which confirmed the radical nature of the product. The EPR spectrum was recorded at room temperature and no hyperfine splitting was observed. Our studies (*vide infra*) suggest that $TAT^{\bullet+}$ is a completely delocalized system and all the nitrogen atoms are equivalent. Hence hyperfine splitting due to the three nitrogen atoms ($I = 1$) would be expected. Since we did not observe any hyperfine structure we can assume that the electron hopping between the sites is very rapid at room temperature. The simulated EPR spectrum (see ESI†) was nearly identical to the experimental spectrum. The EPR spectrum of $TAT^{\bullet+}$ computed using DFT, however shows signatures of hyperfine splitting (see ESI†). Absence of hyperfine splitting also may be due to large numbers of small unresolved splittings which lead to line broadening. Lack of hyperfine splitting and line broadening was noted previously in a few polyphenylenediamine radical cations.[28]

Absorption spectrum of $TAT^{\bullet+}$ in ACN is shown in Fig. 2C. Electronic spectrum in DCM was nearly identical. The absorption band at 690 nm (14 492 cm^{-1}) was assigned to $TAT^{\bullet+}$ absorption and the lower energy band system in the 800–1400 nm (12 500–7000 cm^{-1}) region is assigned to the IV-CT transition. The IV-CT band exhibited vibrational fine structure which is nearly the same in ACN and DCM. We have previously shown that aromatic amines are converted quantitatively to their radical cations by Cu^{2+} in ACN[27] and the extinction coefficients reported in Fig. 2C assume complete conversion of TAT to $TAT^{\bullet+}$. The IV-CT band could be deconvoluted into three Gaussian bands with $\tilde{\upsilon}_{max}$ at 8408, 9692 and 11 042 cm^{-1} (Fig. 2C). The $\Delta\tilde{\upsilon}$ values between the three vibrational peaks are 1284 and 1350 cm^{-1}, which correspond to the IR stretching frequencies of C–N bonds. Fig. 2C also shows the electronic spectrum of $TAT^{\bullet+}$ in ACN computed using TDDFT (B3LYP/6-311G(d,p) level). The computed absorption spectrum is in reasonable agreement with the experimental spectrum. The computed lowest energy peak appears at 9106 cm^{-1}, while the experimental IV-CT band appears at 8546 cm^{-1}.

The $TAT^{\bullet+}$, being a cation is electron deficient and can complex with the parent amine which is electron rich or undergo dimerization as is well known in the case of triarylamine radical cations and it may be argued that the observed absorption spectrum may correspond to some of these species. We rule out these possibilities based on the following: no concentration dependence was observed for the absorption spectrum. We have shown previously that the reaction of aromatic amines with Cu^{2+} is quantitative, even at micromolar concentrations and hence starting amine will not be present when one equivalent of Cu^{2+} is added. In the case of triarylamines we have shown that the radical cations generated from amines using Cu^{2+} dimerize to give benzidine radical cations and the mechanistic aspects of these reactions are described in previous papers.[26,27] We observed that disappearance of the radical cation absorption and formation of IV-CT bands due to benzidine radical cations can be clearly followed by UV-Vis spectroscopy and the reaction requires few minutes for completion. Workup of the reaction mixture in these cases gave the dimer benzidines as products. In the case of the reaction of TAT with Cu^{2+} the absorption spectrum in Fig. 2C was obtained immediately after mixing and no time-dependent changes were noted. Upon workup of the reaction mixture the TAT starting material was recovered. Thus we believe that the absorption spectrum shown in Fig. 2C is due to $TAT^{\bullet+}$ and not due to its aggregated or dimerized derivatives.

The maximum of the lowest energy band in ACN and DCM differs by only 80 cm^{-1}, which shows that the IV-CT band is nearly solvent independent. In the TAT all the three N atoms are equivalent. If $TAT^{\bullet+}$ is a class II IV-CT system, then the positive charge would be localized on one of the nitrogen atoms, making it slightly different from the other two. The solvent dipoles around the positively charged nitrogen will be systematically oriented to stabilize the charge whereas solvent molecules around the other nitrogen atoms would be disordered. The C–$N^{\bullet+}$ bond lengths also will be slightly different from the C–N

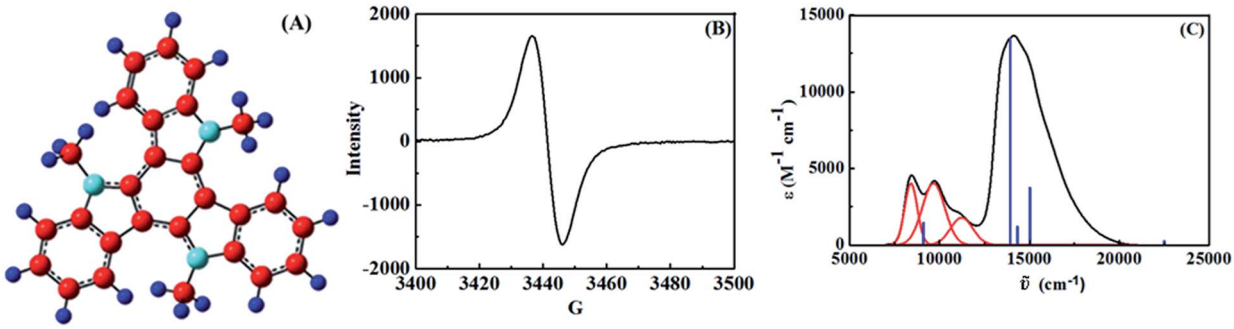

Fig. 2 Optimized geometry (A), EPR (B) and electronic absorption spectra (C) of $TAT^{\bullet+}$ in ACN. In (C) the blue lines represent the computed electronic spectrum and the curves in red are the de-convoluted vibrational bands.

bond lengths. Intervalence charge transfer will lead to shifting of the positive charge to another nitrogen atom and this would require reorganization of the solvent shell and bond lengths around the new and old charge centres. Thus the energy for the optically induced charge transfer (E_{op}) is given by[1]

$$E_{op} = h\tilde{\nu}_{max} = \lambda_o + \lambda_i \quad (1)$$

where h is the Planck's constant, $\tilde{\nu}_{max}$ is the maximum of the IV-CT band, λ_o is the outer shell (or solvent) reorganization energy and λ_i is the inner shell reorganization energy. λ_i arises due to bond length changes associated with the electron transfer and is expected to be solvent independent. λ_o on the other hand is solvent dependent and is given by the equation,

$$\lambda_o = \Delta e^2\,(1/2r_1 + 1/2r_2 - 1/r_{12})(1/\varepsilon_{op} - 1/\varepsilon_s) \quad (2)$$

where the redox centers are assumed to be spherical with radii r_1 and r_2, and a center to center distance of r_{12}, and ε_s and ε_{op} are the optical and static dielectric constants of the solvent. Since the value of λ_o depends on the solvent polarity, energy of the IV-CT absorption will change with solvent as per eqn (1) for a class II system.

Upon going from a class II to class III system the electronic coupling increases making $\lambda_i > \lambda_o$ resulting in the elimination of solvent barrier to electron transfer. This means that the solvent configuration of the donor and acceptor states will be averaged and solvent reorganization will no longer contribute to E_{op}. Thus the IV-CT band of a class III system is expected to be solvent independent. The absence of solvent dependence in the class III system can be explained in another way also. In this system the minima of the ground and excited state free energy surfaces are at the same point in the ET coordinate. Optical excitation takes the electron from the bottom of the ground state surface to the bottom of the excited state surface. The difference in the ground state and excited state dipole moments is zero and hence the excitation is not associated with any charge transfer. The optical absorption involves transition between delocalized molecular orbitals of the system and the transition should not show any solvent dependence.

The vibrational fine structure in the IV-CT band and its solvent independent nature suggest that $TAT^{\bullet+}$ is a Robin and Day class III system.[1,2] Hush has shown that the band-width ($\tilde{\nu}_{1/2}$) of the IV-CT band is given by $\tilde{\nu}_{1/2} = 47.94\sqrt{\tilde{\nu}_{max}}$, and if the observed band-width is much lower than that calculated by the above equation, the system would belong to class III.[4,5] In the case of $TAT^{\bullet+}$ the $\tilde{\nu}_{1/2}$ observed (2671 cm^{-1}) was much smaller compared to the calculated value (4431 cm^{-1}), further supporting the assignment of $TAT^{\bullet+}$ as a class III system. In class III systems the coupling between the redox centers is so strong that the system is completely delocalized and intermediate valence states have to be attributed to the redox centers. In the case of $TAT^{\bullet+}$ this means that all the three N atoms share the positive charge equally and exchange is very fast.

TAT has three redox active centers arranged in a non-linear fashion and hence it is to be regarded as a multidimensional IV-CT system.[29–32] Although several organic multidimensional IV-CT systems including derivatives of TAB were studied in the past, none of them were found to belong to class III, and the $TAT^{\bullet+}$ reported here is the first example of a stable, multidimensional class III IV-CT system. The two-center model for IV-CT is very well known, but three-center (or tri-nuclear) models are less frequently encountered. A semi-classical model to describe the potential energy surfaces (PES) in such systems was earlier proposed by Launay and Babonneau (LB model),[33] subsequent to which Cannon *et al.* (Cannon model)[34] reported an alternative approach to obtain the PES. Here, we employ both the models to describe the PES of $TAT^{\bullet+}$. A change in oxidation state at a single site of the tri-nuclear system results in a modification of the corresponding bond lengths at the site. The vibrational breathing modes corresponding to such a deformation are considered harmonic in the LB and the Cannon models. The interactions of the zero-order diabatic states are considered within the first-order perturbation theory formalism to generate the adiabatic states of the system. The energies of the adiabatic states are obtained as solutions to the three-state secular determinant. In the LB model, the behaviour of the tri-nuclear system is described by a single dimensionless parameter '*B*', which is a measure of the competition between the electronic interaction favouring delocalization and the electron–phonon interaction favouring localization. Absence of electronic coupling between the nitrogen centers in $TAT^{\bullet+}$ corresponds to a situation where the value of the '*B*' parameter is zero. For such a situation, the contours of the PES have been obtained and are shown in Fig. 3. Note that the energies and the coordinates are represented in reduced units (see eqn (1) of ref. 33) and the contours are shown in the (q_2, q_3) plane.

An explicit way of obtaining the diabatic and the adiabatic potential energy curves has been outlined by the Cannon model. In their approach, the electronic coupling is described by the parameter '*c*'. It has to be noted that the '*c*' parameter is equivalent to '3*B*' in the LB model. The diabatic, and the adiabatic potential energy curves (in reduced units; see ref. 34 for further details) corresponding to $c = 0$ are obtained using the Cannon model and these are shown in Fig. 4. It can be seen from Fig. 4 that the diabatic state potential energy curves are retrieved from the adiabatic states for the $c = 0$ case. The individual potential energy curves are shown in ESI† for the sake of clarity.

For a class III system, the energy of the IV-CT optical transition (E_{op}) is given by three times the magnitude of the electronic coupling matrix element between the diabatic states.

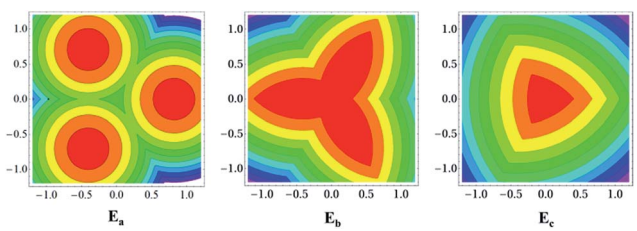

Fig. 3 Potential energy contours as a function of the nuclear co-ordinates for the adiabatic states of $TAT^{\bullet+}$ when $B = 0$ (localization).

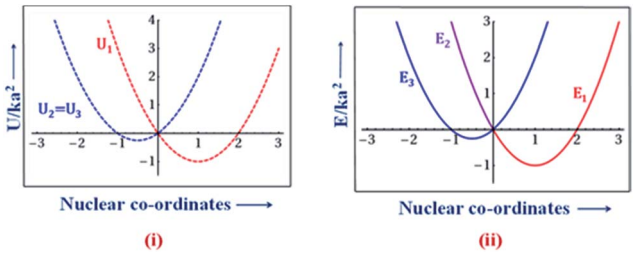

Fig. 4 Potential energy curves as a function of the nuclear co-ordinates for (i) the diabatic states (U_1, U_2 and U_3) and (ii) the adiabatic states (E_1, E_2 and E_3) of $TAT^{\bullet+}$ for $c = 0$ (localization).

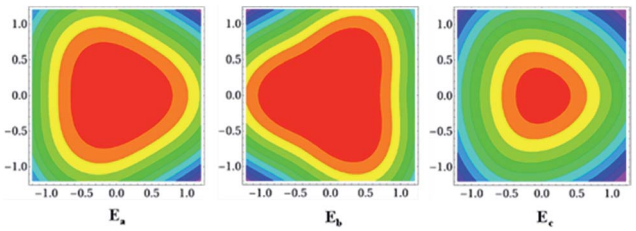

Fig. 5 Potential energy contours as a function of the nuclear co-ordinates for the adiabatic states of $TAT^{\bullet+}$ when $B = -0.41$ (delocalization).

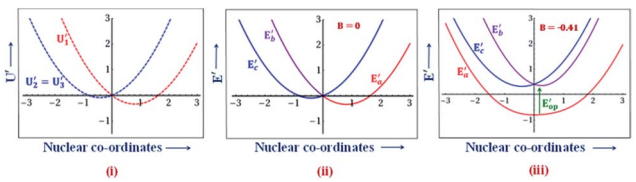

Fig. 6 Potential energy curves as a function of the nuclear co-ordinates for (i) the diabatic states (U'_1, U'_2 and U'_3) and the adiabatic states (E'_a, E'_b and E'_c) of $TAT^{\bullet+}$ for (ii) $B = 0$ (localization) and (iii) $B = -0.41$ (delocalization). E'_{op} is the energy of the IV-CT optical transition in reduced units.

Therefore, in the notation of the Cannon model, $E_{op} = 3|\beta|$. For $TAT^{\bullet+}$ the 0–0 of the intervalence band occurs at 8546 cm^{-1}. Since $|\beta| = E_{op}/3$, the magnitude of the electronic coupling turns out to be 2848.67 cm^{-1} (=0.353 eV). Within the framework of the Cannon model, $c = \beta/ka^2$, where 'k' $= f/3$, 'f' is the force constant and 'a' is the deformation in the M–X distance. The numerical value of the force constant, 'f' was chosen to be 26.33 eV $Å^{-2}$ in our calculations on $TAT^{\bullet+}$, corresponding to the frequency of the breathing vibrational mode obtained from the electronic structure calculations (see ESI†). This vibrational mode frequency is in the range of aromatic C–N stretch mode. The value of 'a' was chosen to be 0.18 Å (difference between the C–N and C=N bond lengths).[35] We thus evaluate the numerical value of 'c' and find it to be −1.24. This corresponds to a 'B' value of −0.41 in the LB model. For $TAT^{\bullet+}$, we obtained the PES contours for $B = -0.41$ and these are shown in Fig. 5.

Adiabatic potential energy curves can then be obtained by performing a transformation from the (q_2, q_3) variables to the (r, θ) variables and then taking a cross-section of the resultant surfaces in the $\theta = 0$ plane.[34] The resultant potential energy matrix thus obtained was diagonalized for a given value of 'B' to obtain the adiabatic potential energy curves. Thus, for $TAT^{\bullet+}$ ($B = -0.41$), the adiabatic curves are obtained and are shown in Fig. 6. The energies are reported as E′ in reduced units. Note that, for a comparison, we also show the diabatic and the adiabatic states for the $B = 0$ case in the same figure. We believe that these PES best describe the electron delocalization in $TAT^{\bullet+}$.

Conclusions

For two-center class III IV-CT systems, very large electronic coupling energies were reported as in the case of tetramethyl-*p*-phenylenediamine$^{\bullet+}$ (1.02 eV), tetraphenyl-*p*-phenylenediamine$^{\bullet+}$ (0.75 eV), tetramethylbenzidine$^{\bullet+}$ (0.61 eV) and phenylene-bridged bis(dioxaborine)$^{\bullet-}$ (0.68 eV).[36,37] The electronic coupling energy obtained for $TAT^{\bullet+}$ is only 0.35 eV. Lambert and Nöll have reported coupling energy as high as 0.40 eV for class II/class III borderline cases.[38] Under these circumstances some caution needs to be exercised in classifying $TAT^{\bullet+}$ as a completely delocalized class III system, as no trigonal class III systems are reported so far in the literature. The following factors strongly support our assignment. The absorption spectrum of $TAT^{\bullet+}$ exhibited negligible solvent dependence. The clear vibrational structure in the IV-CT spectrum is also a strong indication of class III behaviour. Launay and Babonneau have predicted that for trinuclear systems the third redox center would favorably influence the delocalization process leading to the observation of the class II/class III transition at much lower coupling energies.[33] Using the coupling energy of 0.35 eV for $TAT^{\bullet+}$ we calculated the 'c' parameter of the Cannon model as −1.24 and the 'B' parameter of the LB model as −0.41. The Cannon model predicts class III behavior at $c < -0.7611$ and the LB model predicts class III behavior for $B < -0.25$. Thus both models also predict that $TAT^{\bullet+}$ would belong to class III and one can use $TAT^{\bullet+}$ to verify the predictions of both the LB and the Cannon models for three-center systems.

Acknowledgements

TGT thanks Ms. J. Sridevi, CSIR-Central Leather Research Institute, Chennai for EPR measurements and CSIR for financial support. SCS and RSS thank IISER-TVM for computational facilities and financial support. The authors thank Abbey M. Philip for suggesting the possibility of simulating EPR using EasySpin.

References

1 A. Heckmann and C. Lambert, *Angew. Chem., Int. Ed.*, 2012, **51**, 326–392.
2 J. Hankache and O. Wenger, *Chem. Rev.*, 2011, **111**, 5138–5178.
3 C. Creutz, M. D. Newton and N. Sutin, *J. Photochem. Photobiol., A*, 1994, **82**, 47–59.

4 N. S. Hush, *Coord. Chem. Rev.*, 1985, **64**, 135–157.
5 N. S. Hush, *Electrochim. Acta*, 1968, **13**, 1005–1023.
6 J. H. Heo, S. H. Im, J. H. Noh, T. N. Mandal, C.-S. Lim, J. A. Chang, Y. H. Lee, H.-j. Kim, A. Sarkar, M. K. Nazeeruddin, M. Gratzel and S. I. Seok, *Nat. Photonics*, 2013, **7**, 486–491.
7 Z. Jiang, T. Ye, C. Yang, D. Yang, M. Zhu, C. Zhong, J. Qin and D. Ma, *Chem. Mater.*, 2011, **23**, 771–777.
8 P. Gratia, A. Magomedov, T. Malinauskas, M. Daskeviciene, A. Abate, S. Ahmad, M. Grätzel, V. Getautis and M. K. Nazeeruddin, *Angew. Chem., Int. Ed.*, 2015, **54**, 11409–11413.
9 N. J. Jeon, H. G. Lee, Y. C. Kim, J. Seo, J. H. Noh, J. Lee and S. I. Seok, *J. Am. Chem. Soc.*, 2014, **136**, 7837–7840.
10 H. Nishimura, N. Ishida, A. Shimazaki, A. Wakamiya, A. Saeki, L. T. Scott and Y. Murata, *J. Am. Chem. Soc.*, 2015, **137**, 15656–15659.
11 A. Wakamiya, H. Nishimura, T. Fukushima, F. Suzuki, A. Saeki, S. Seki, I. Osaka, T. Sasamori, M. Murata, Y. Murata and H. Kaji, *Angew. Chem., Int. Ed.*, 2014, **53**, 5800–5804.
12 H. Li, K. Fu, A. Hagfeldt, M. Grätzel, S. G. Mhaisalkar and A. C. Grimsdale, *Angew. Chem., Int. Ed.*, 2014, **53**, 4085–4088.
13 T. Bura, N. Leclerc, S. Fall, P. Lévêque, T. Heiser and R. Ziessel, *Org. Lett.*, 2011, **13**, 6030–6033.
14 Q. Ye, J. Chang, J. Shao and C. Chi, *J. Mater. Chem.*, 2012, **22**, 13180–13186.
15 E. M. García-Frutos and B. Gómez-Lor, *J. Am. Chem. Soc.*, 2008, **130**, 9173–9177.
16 E. M. García-Frutos, G. Hennrich, E. Gutierrez, A. Monge and B. Gómez-Lor, *J. Org. Chem.*, 2010, **75**, 1070–1076.
17 J. Shao, Z. Guan, Y. Yan, C. Jiao, Q.-H. Xu and C. Chi, *J. Org. Chem.*, 2011, **76**, 780–790.
18 W. Y. Lai, Q. Y. He, R. Zhu, Q. Q. Chen and W. Huang, *Adv. Funct. Mater.*, 2008, **18**, 265–276.
19 F. J. Ramos, K. Rakstys, S. Kazim, M. Gratzel, M. K. Nazeeruddin and S. Ahmad, *RSC Adv.*, 2015, **5**, 53426–53432.
20 X. Qian, Y.-Z. Zhu, J. Song, X.-P. Gao and J.-Y. Zheng, *Org. Lett.*, 2013, **15**, 6034–6037.
21 S. W. Shelton, T. L. Chen, D. E. Barclay and B. Ma, *ACS Appl. Mater. Interfaces*, 2012, **4**, 2534–2540.
22 C. Ruiz, E. M. García-Frutos, D. A. da Silva Filho, J. T. López Navarrete, M. C. Ruiz Delgado and B. Gómez-Lor, *J. Phys. Chem. C*, 2014, **118**, 5470–5477.
23 K. R. Stickley and S. C. Blackstock, *Tetrahedron Lett.*, 1995, **36**, 1585–1588.
24 L. Ginnari-Satriani, V. Casagrande, A. Bianco, G. Ortaggi and M. Franceschin, *Org. Biomol. Chem.*, 2009, **7**, 2513–2516.
25 M. Franceschin, L. Ginnari-Satriani, A. Alvino, G. Ortaggi and A. Bianco, *Eur. J. Org. Chem.*, 2010, **2010**, 134–141.
26 K. Sreenath, C. Suneesh, K. Gopidas and R. Flowers, *J. Phys. Chem. A*, 2009, **113**, 6477–6483.
27 S. Sumalekshmy and K. R. Gopidas, *Chem. Phys. Lett.*, 2005, **413**, 294–299.
28 K. R. Stickley, T. D. Selby and S. C. Blackstock, *J. Org. Chem.*, 1997, **62**, 448–449.
29 J. Bonvoisin, J.-P. Launay, W. Verbouwe, M. Van der Auweraer and F. C. De Schryver, *J. Phys. Chem.*, 1996, **100**, 17079–17082.
30 J. Bonvoisin, J.-P. Launay, M. Van der Auweraer and F. C. De Schryver, *J. Phys. Chem.*, 1996, **100**, 18006.
31 J. Sedó, D. Ruiz, J. Vidal-Gancedo, C. Rovira, J. Bonvoisin, J.-P. Launay and J. Veciana, *Adv. Mater.*, 1996, **8**, 748–752.
32 Y. Hirao, A. Ito and K. Tanaka, *J. Phys. Chem. A*, 2007, **111**, 2951–2956.
33 J. P. Launay and F. Babonneau, *Chem. Phys.*, 1982, **67**, 295–300.
34 R. D. Cannon, L. Montri, D. B. Brown, K. M. Marshall and C. M. Elliott, *J. Am. Chem. Soc.*, 1984, **106**, 2591–2594.
35 www.chem.tamu.edu/rgroup/connell/linkfiles/bonds.pdf.
36 C. Risko, S. Barlow, V. Coropceanu, M. Halik, J.-L. Bredas and S. R. Marder, *Chem. Commun.*, 2003, 194–195, DOI: 10.1039/b210429f.
37 S. F. Nelsen, H. Q. Tran and M. A. Nagy, *J. Am. Chem. Soc.*, 1998, **120**, 298–304.
38 C. Lambert and G. Nöll, *J. Am. Chem. Soc.*, 1999, **121**, 8434–8442.